Chlamydomonas reinhardtii Metabolic Pathway Analysis for Biohydrogen Production under Non-Steady State Operation

Dongda Zhang and Vassilios S. Vassiliadis*

E-mail: vsv20@cam.ac.uk

Phone: +44 (0) 1223 330142. Fax: +44 (0) 1223 334796

Abstract

This paper presents a novel structured dynamic model to simulate the metabolic reaction network of green algae hydrogen production from aerobic condition to anaerobic condition, which has not been addressed in the open literature to this date. An efficient parameter estimation methodology is proposed to avoid the difficulty of measuring essential kinetic parameters from experiments. The accuracy of the model is verified by comparison to published experimental results. The current model finds that the starch generation pathway mainly competes with hydrogen production pathway, as its activity is enhanced by the cyclic electron flow pathway. From the dynamic sensitivity analysis, it is concluded that the most effective solution to enhance hydrogen production is to seek the optimal sulphur concentration in the culture, rather than to modify the activity of specific enzymes. The current work also denies the previous hypothesis that the diffusion of small proteins in the metabolic network inhibits hydrogen production.

*To whom correspondence should be addressed

1 Introduction

The major component leading to global warming is carbon dioxide, CO_2, which is mainly released by burning fossil-based fuels such as petrol, coal and natural gas[1]. To reduce the production of CO_2 and fulfill the increasing demand for energy production, seeking novel sustainable and environmental friendly energy sources has become a key research target internationally.

Recently, hydrogen has been considered as a replacement to traditional energy sources due to its high combustion heat with zero environmental impact. It has been estimated that the requirement of hydrogen as a fuel for transportation will increase from 5.4 million tonnes in 2025 to 100 millions in 2050 worldwide[2]. However, the present industrial hydrogen generation processes mainly rely on the utilisation of non-renewable carbon based resources. To find alternatives to conventional hydrogen sources, developments in the field of sustainable hydrogen energy have led to renewed interest in biohydrogen production. Biohydrogen is produced by microorganisms such as photosynthetic bacteria and green algae.

The most attractive advantage of using microorganisms is that they can utilise solar energy and assimilate organic acids or CO_2 for biohydrogen production[1,3]. Because of the availability and low investment cost of energy and carbon sources, biohydrogen production is regarded as a feasible and sustainable process to replace current hydrogen production processes.

1.1 Important metabolic pathways

Since Melis et al.[4] discovered that hydrogen can be produced by *Chlamydomonas reinhardtii*, a type of green algae, in anaerobic circumstances, intense research[5,6] has been carried out to determine the metabolic pathways of hydrogen production in this species. At present, it is widely accepted that *C. reinhardtii* can generate hydrogen via three different mechanisms: (a) the PSII (photosystem II) independent pathway, (b) the PSII dependent pathway and (c) the dark fermentative pathway[7].

Among the three metabolic pathways, the PSII dependent metabolic pathway is particularly

studied since it supplies most of the electrons for hydrogen production in the light photosynthetic fermentation process[7,8]. Photosystem II, a large protein complex in chloroplasts and containing the reaction center of P_{680}, can can extract electrons from water molecules by utilising solar energy[6]. Once electrons are extracted from water, they are transferred through different electron carriers including plastoquinone (PQ) in the PQ pool, cytochrome protein complex (Cyt b_6f) and plastocyanin (PC), and eventually sent to photosystem I (PSI), a large protein complex containing the reaction center of P_{700}. To replenish the energy loss of electrons during the transfer from PSII to PSI, PSI harvests solar energy to excite the exhausted electrons. Electrons are thereby delivered to ferredoxin (Fd). Finally, the reduced Fd is oxidised by hydrogen ions for molecular hydrogen generation, and this reaction is catalysed by an enzyme named hydrogenase (HydA)[5,7]. Figure 1 shows the process of the PSII dependent metabolic pathway.

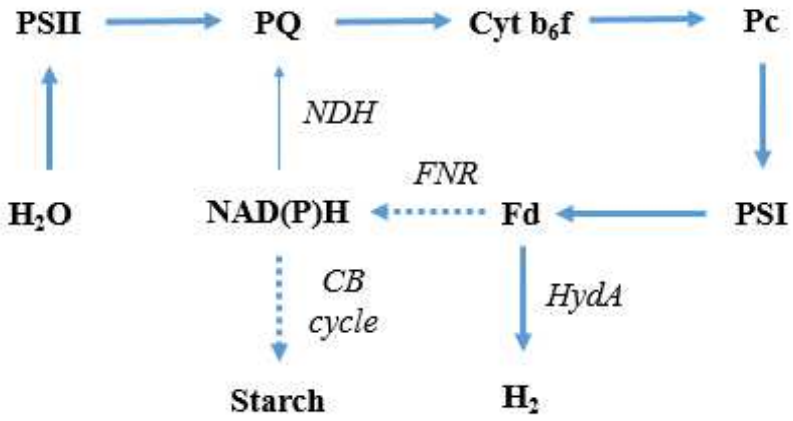

Figure 1: Illustration of different electron transfer pathways. Thick lines show the PSII dependent hydrogen production pathway, dashed lines show the starch generation pathway, thin lines show the cyclic electron flow pathway. PSII represents photosystem II, PQ represents plastoquinone, Cyt b_6f represents cytochrome b_6f, PC represents plastocyanin, PSI represents photosystem I, Fd represents ferredoxin, HydA represents hydrogenase, NDH represents NAD(P)H dehydrogenase enzyme, and FNR represents ferredoxin-NADP-reductase.

The PSII dependent metabolic pathway is only active in anaerobic conditions due to the strong inhibition of oxygen on hydrogenase activity. When oxygen is present, the hydrogen generation pathway is replaced by the general photosynthetic process, named as the

CO_2 fixation pathway (starch generation pathway, shown in Figure 1). In this pathway, the reduced Fd donates electrons to $NAD(P)^+$ with the help of another enzyme, ferredoxin-NADP-reductase (FNR), and then NAD(P)H (reduced $NAD(P)^+$) passes electrons to the Calvin-Benson cycle for CO_2 fixation (starch generation)[7]. Both the starch generation pathway and the hydrogen production pathway are entitled as linear electron flow (LEF).

One feasible method to create the anaerobic condition is to use a sulphur deprived culture[9]. As sulphur is essential for PSII repair, the lack of intracellular sulphur can lead to a dramatic decrease on photosynthetic activity since PSII contains the reaction center for water decomposition and its activity is markedly depressed.

Melis et al.[4] claimed that the residual photosynthetic activity of algae in a sulphur-free culture will significantly drop to less than 20% of its original activity within the first 40 hours of cultivation. Oxygen produced by photosynthesis thereby is totally consumed by algae due to the their high respiration rate.

Furthermore, a sulphur-free culture can aggravate the degradation of ribulose 1,5-bisphosphate carboxylase (Rubisco), an essential enzyme for CO_2 fixation[9]. Hence, the activity of the starch generation pathway is significantly suppressed[8]. As a result, hydrogen ions become the major electron sink consuming the electrons generated through the LEF pathway.

Cyclic electron flow (CEF) (Figure 1) is another photosynthesis pathway simultaneous with LEF pathways. In the CEF pathway, electrons in PSI are activated by light and transferred to the PQ pool via ferredoxin and $NAD(P)^+$. To accomplish the cycle, electrons at the PQ pool are sent back to PSI through the same chain in LEF pathway. The distinctive characteristic of CEF pathway is that this pathway only generates ATP but not electrons. There is no net generation of electrons since they are trapped in the cyclic electron transfer chain.

LEF pathway is the major photosynthesis pathway in aerobic circumstances, and the CEF pathway becomes the major photosynthetic pathway in anaerobic conditions[10]. Another hypothetical mechanism of the CEF pathway is that ferredoxin immediately transfers electrons

to the PQ pool via ferredoxin-quinone-reductase (FQR), without the attendance of FNR[7]. However, so far there is no research available that is able to identify or isolate FQR, and a recent study has demonstrated that there is no unidentified protein involved in the CEF pathway[11]. Therefore, this unproven mechanism is not included in the current research.

The transport of hydrogen ions between the lumen side and the stroma side of chloroplasts is another important step involved in both LEF and CEF pathways[7]. Hydrogen ions at the stroma side participate the electron transfer step from the PQ pool to Cyt b_6f, and are pumped to the lumen side at the meanwhile. Hydrogen ions at the lumen side come back to the stroma side with the formation of ATP by ATPase. At the stroma side, hydrogen ions are consumed for the generation of either starch or hydrogen depending on the culture circumstances. Because of the important role of hydrogen ions during the electron transfer process, the hydrogen production rate can be suppressed if hydrogen ions at the stroma side are not sufficient[12,13].

1.2 Simulation of metabolic reaction network

A number of research articles have been published investigating the metabolic constraints of green algal hydrogen production by designing different experiments[14–18]. However, as the activity of most metabolic pathways continuously changes during the hydrogen production period, the effect of each metabolic pathway on hydrogen production is different at each time. It is therefore time-consuming to determine all of the potential metabolic constraints for algal hydrogen production purely by experiments. As a result, simulation becomes a valuable tool to identify the change of activity of metabolic pathways, and the interactions of different reactions in the metabolic network of algal hydrogen production.

Diverse simulation methods have been developed to model different metabolic reaction networks. Among these methods, flux balance analysis (FBA) and dynamic simulation are most prominent. For example, previous research reconstructed the metabolic network of different microorganisms by FBA[19,20]. The major metabolic pathways of microorganisms under different circumstances are also determined by FBA[21,22]. Dynamic simulation is mainly used

to model the fermentation process of bioproducts manufacture[23–26]. It is also applied to simulate the dynamic period of metabolic pathways[16].

1.2.1 Flux balance analysis

Generally, FBA can be described as below[27].

$$\max_{v} c^T v \tag{1a}$$

subject to:

$$Mv = 0 \tag{1b}$$

$$\alpha_i \leq v_i \leq \beta_i \tag{1c}$$

$$i = 1, 2, \ldots, NE$$

where v is the metabolite concentration vector, c is the objective function coefficient vector, M is the stoichiometric matrix, v_i is the concentration of metabolite i, α_i and β_i are the lower bound and upper bound of metabolite i.

As FBA is based on the assumption that the metabolic reaction network is under steady state, there is no net accumulation of any metabolite. The concentration of each metabolite is kept constant and the mass balance of metabolites can be written by Equation (1b).

In general, the solution of Equation (1b) are not unique as the number of metabolites is larger than the rank of the stoichiometric matrix M. Equation (1a) (objective function) thereby is used to ascertain a particular metabolic reaction rates distribution and determine the single solution of Equation (1b). The objective function in FBA is the hypothesised good of the microorganism: usually to maximise the synthesis of bioproducts and to minimise the consumption of energy and nutrients[19]. Equation (1c) represents the range of metabolite concentrations.

The significant advantage of FBA is that this method does not rely on any reaction kinetics, facilitating its wide application in the reconstruction of large metabolic networks and the identification of metabolic bottlenecks. However, this method is not valid for a dynamic

reaction network due to the steady-state assumption. Furthermore, as FBA does not contain reaction kinetics it cannot be utilised to seek the limiting reaction steps in a metabolic network.

1.2.2 Dynamic simulation

Dynamic simulation consists of both reaction kinetics and mass balances of metabolites. Reaction kinetics can be expressed by different functional forms. For example, Equation (2a) shows the Michaelis–Menten kinetics and Equation (2b) shows the power law function. The mass balance of metabolites is shown as Equation (2c).

$$r_i = V_{\max} \cdot \prod_{j=1}^{N_{i,j}} \frac{c_j}{K_{i,j} + c_j} \tag{2a}$$

$$r_i = k_i \cdot \prod_{j=1}^{N_{i,j}} c_j^{n_{i,j}} \tag{2b}$$

$$\frac{dc_j}{dt} = \sum_{i=1}^{n} r_i \cdot x_{i,j} \tag{2c}$$

where k_i represents the reaction rate constant of reaction i, $N_{i,j}$ represents the number of metabolites involved in reaction i, $n_{i,j}$ represents the exponential index of metabolite j in reaction i, c_j represents the concentration of metabolite j, $K_{i,j}$ represents the kinetic parameter in Michaelis–Menten equation, $V_{\max}$ represents the highest reaction rate of reaction i, n represents the number of reactions, $x_{i,j}$ represents the stoichiometry of metabolite j in reaction i.

Compared to FBA, dynamic simulation requires reaction kinetics which are usually difficult to estimate. Therefore, this method is not suitable for the simulation of large scale metabolic networks. However, dynamic simulation is able to determine the limiting reaction steps and competing metabolic pathways for bioproduct synthesis. It is also capable of modelling a dynamic metabolic process where the principle of FBA is not valid.

Specific to the current study, the activity of the LEF and CEF pathways continuously changes

due to the decreasing intracellular sulphur concentration, and the culture operation switches from the aerobic condition to the anaerobic condition. Therefore the current metabolic reaction network is not under steady-state. Furthermore, the current research aims to determine the limiting reaction steps in the hydrogen generation pathway and the major competing pathway for hydrogen production. For these reasons, the dynamic simulation method is eventually selected in the present study.

2 Methodology of model construction

2.1 Dynamic model for metabolic network

A dynamic model consists of reaction kinetics and mass balance. The indispensable information for model construction includes the kinetic parameters of each reaction and the initial concentration of each metabolite. However, these data are always hard to know due to the difficulty of *in-vivo* intracellular metabolite concentration measurement. Even though many reaction kinetics have been measured by *in-vitro* experiments, the significant different biological circumstances between *in-vitro* and *in-vivo* tests may lead to large errors. To solve the problem of kinetic data shortage, the current research proposes a novel method to estimate kinetic parameters. To illustrate the proposed methodology, the dynamic model for the algal hydrogen production metabolic network is shown from Section 2.1.1 to Section 2.1.4 as an example.

2.1.1 Metabolic pathways

The metabolic pathways included in the current model are: (1) the hydrogen generation pathway, (2) the cyclic electron flow pathway (CEF), (3) the starch generation pathway, and (4) the transport of hydrogen ions between the lumen side and the stroma side of chloroplasts. Both pathway (1) and pathway (3) can be named as the LEF pathway, since they share the same electron transfer chain from PSII to Fd as shown in Figure 1. The detailed reaction steps in each pathway are listed in the Appendix.

2.1.2 Initial concentration of proteins

The initial concentration of photosynthetic proteins including PSI, PQ, PC, Cyt b_6f and Fd has to be determined. Although there are only 5 types of proteins, each protein includes at least two states, which are the oxidised state and the reduced state. Some proteins such as PQ and Cyt b_6f even have up to 6 or 7 different states due to the complicated reaction mechanisms in the electron transfer chain[16].

Since previous research[4,28–34] only measured the total concentration of each type of protein, the current research assumes that the different states of each protein have the same initial intracellular concentration. This assumption is partially supported by previous work which measured the concentration of some photosynthetic proteins at different states and found they are very similar[35]. The initial concentration of each protein in the current model is shown in Table 1. The impact of the initial concentration of the proteins involved can be measured by initial condition dynamic sensitivity analysis treating them as parameters, and this is shown in Section 3.5.

Table 1: Initial values of current model. $c_{O_2,0}$, X_0 and Q_0 are obtained from[24], and initial concentration of metabolites are obtained from[4,28–34].

Material	Initial value	Unit	Material	Initial value	Unit
PSI	2.3	$\text{amol} \cdot \text{cell}^{-1}$	PC	4.5	$\text{amol} \cdot \text{cell}^{-1}$
PSI^+	2.3	$\text{amol} \cdot \text{cell}^{-1}$	PC^+	4.5	$\text{amol} \cdot \text{cell}^{-1}$
fb	0.75	$\text{amol} \cdot \text{cell}^{-1}$	Fd^+	0.6	$\text{amol} \cdot \text{cell}^{-1}$
$\text{fb} \cdot \text{PQ}$	0.75	$\text{amol} \cdot \text{cell}^{-1}$	Fd	0.6	$\text{amol} \cdot \text{cell}^{-1}$
$[\text{fb} \cdot \text{PQ}]^+$	0.75	$\text{amol} \cdot \text{cell}^{-1}$	H_2	0	$\text{amol} \cdot \text{cell}^{-1}$
$[\text{fb} \cdot \text{PQH}]$	0.75	$\text{amol} \cdot \text{cell}^{-1}$	$[CH_2O]$	0.3×10^6	$\text{amol} \cdot \text{cell}^{-1}$
$\text{fb} \cdot \text{PQH}_2$	0.75	$\text{amol} \cdot \text{cell}^{-1}$	NAD^+	12	$\text{amol} \cdot \text{cell}^{-1}$
$[\text{fb} \cdot \text{PQH}]^+$	0.75	$\text{amol} \cdot \text{cell}^{-1}$	NADH	12	$\text{amol} \cdot \text{cell}^{-1}$
PQ	2.63	$\text{amol} \cdot \text{cell}^{-1}$	$H_L{}^+$	0.05	$\text{amol} \cdot \text{cell}^{-1}$
PQH_2	2.63	$\text{amol} \cdot \text{cell}^{-1}$	$H_S{}^+$	0.05	$\text{amol} \cdot \text{cell}^{-1}$
$c_{O_2,0}$	0.009	$\text{g} \cdot \text{L}^{-1}$	X_0	0.26	$\text{g} \cdot \text{L}^{-1}$
Q_0	5	$\text{mgS} \cdot \text{gX}^{-1}$			

2.1.3 Kinetic constants in the reaction network

Most reactions in the present metabolic network are induced by electrostatic force, and their

kinetics can be expressed in Equation (3). Other reactions which involve the participation of enzymes can be described by Equation (2a).

$$r_i = k_i \prod_j c_j \tag{3}$$

In the current model, only reactions catalysed by NDH, FNR and HydA are expressed by Equation (2a). Because the value of $K_{i,j}$ in these specific reactions is much higher than the concentration of the corresponding substrate[17,36], Equation (2a) can be approximately simplified to Equation (3). As a result, in the current model all of the reaction kinetics are expressed by Equation (3).

To avoid the difficulty of measuring kinetic parameters purely from experiments, a novel method is proposed in the current research to estimate the kinetic constant of each reaction. The procedure is explained below:

1. Find a condition where the current metabolic network is under steady-state;
2. Calculate the number of independent reactions in the metabolic network (number of reactions - rank of stoichiometric coefficient matrix);
3. Choose the reactions which can be easily measured as the independent reactions, and then measure the reaction rate of these reactions;
4. Calculate the reaction rate of other reactions;
5. Find the concentration of each protein under the same steady-state from published literature;
6. Calculate the kinetic constant of each reaction by Equation (3);
7. Use switch functions to simulate the change of reaction rates when the culture condition is changed.

In the current research, the metabolic network can be assumed as steady-state when the culture is aerobic and nutrient-sufficient, as cells can grow healthily in these conditions. The number of independent reactions is equal to 2: the water-splitting reaction (Equation (11a) in the Appendix) in the LEF pathways, and the PSI reduction reaction in the CEF pathway (Equation (12h) in the Appendix) are chosen as the independent reactions since their reaction rates have been accurately measured[4,10,12]. The initial concentration of each protein in the sulphur-sufficient culture has also been measured and shown in Table 1.

The kinetic constants in the current research thereby can be estimated by processing the estimation method outlined above. The detailed kinetic equation of each reaction step and the mass balances of metabolites are shown in the Appendix.

2.1.4 Discrete event modelling

The kinetics of metabolic pathways in micro-organic cells change fast due to the sudden change of culture conditions. For example, when sulphur is depleted the starch generation pathway is suppressed and the hydrogen production pathway is stimulated. The activity of the CEF pathway is also enhanced as it can generate a significant amount of photosynthetic ATP for cell maintenance. However, the regulation of these reaction rates is accomplished by a complicated biological control system, and is quite difficult to represent by mathematical equations.

A discrete model thus is constructed to simplify the complex cellular regulation system. Switch functions, which are similar to the Heaviside step-function but are differentiable, are utilised because they are capable of providing smooth changes when reactions are terminated or started due to a sudden change of the environment. In particular, the switch function selected in the present work is formulated as Equation (4) and its plot is shown in Figure 2.

$$f(x) = 0.5 \cdot \left(1 + \frac{x}{\sqrt{x^2 + \gamma^2}}\right) \tag{4}$$

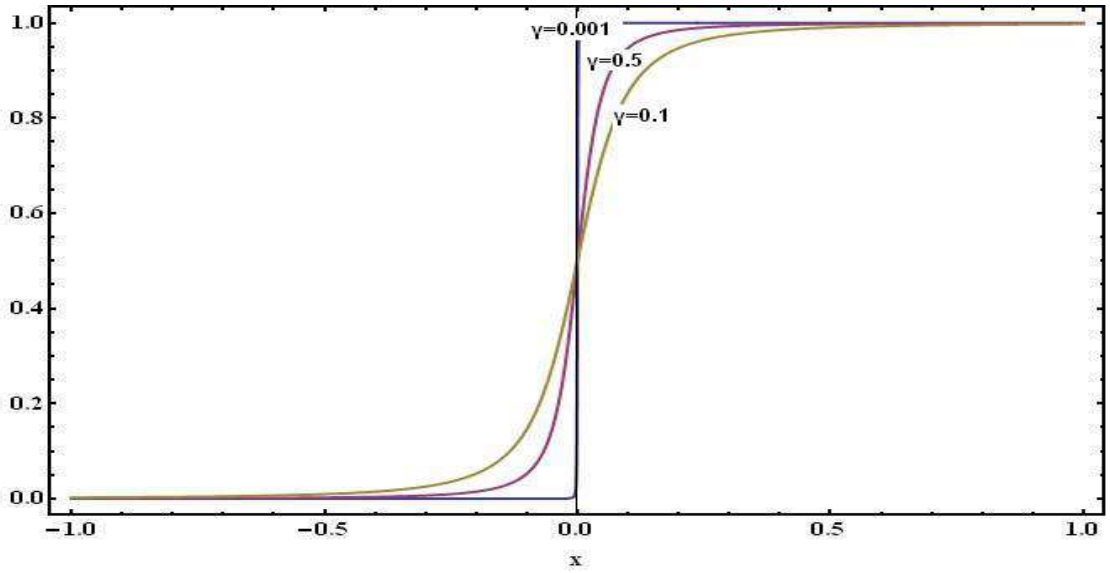

Figure 2: Illustration of the switch function. When $x \geq 0$, $f(x) = 1$; otherwise $f(x) = 0$. The sharpness factor γ in the current study is selected as 0.1 so that the transition from aerobic condition to anaerobic condition is rapid.

Switch functions can also help to avoid a negative concentration when the consumption rate of a substrate does not depend on its concentration. For example, although the consumption rate of oxygen due to algal respiration is a function of oxygen concentration in the culture, the expression of cell respiration rate does not include oxygen concentration in general. Therefore, a negative oxygen concentration may be induced numerically after the time when oxygen concentration drops to zero (Figure 3). To avoid negative oxygen concentrations, a switch function is applied to block the oxygen consumption rate (set it to zero) once oxygen is totally consumed.

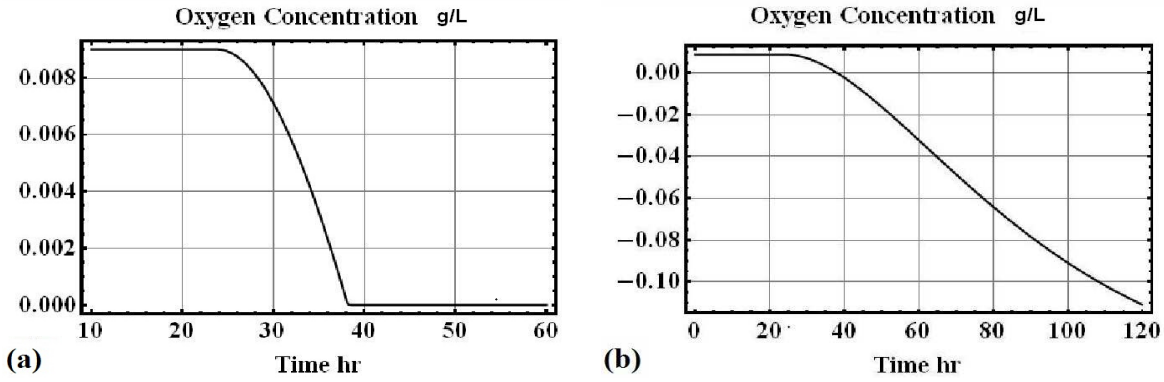

Figure 3: Simulated oxygen concentration at different conditions. (a) oxygen concentration when switch function is added; (b) oxygen concentration when switch function is excluded.

2.2 Dynamic model for algal growth

The water-splitting reaction in both starch and hydrogen generation pathways is catalysed by PSII whose activity is determined by the intracellular sulphur concentration. As the culture for algal hydrogen production is sulphur-free, the consumption rate of intracellular sulphur concentration is totally determined by cell growth rate. The time to switch the culture from aerobic condition to anaerobic condition is also dependent on cell growth rate, as the oxygen consumption rate is affected by biomass concentration. Therefore, it is important to include algal growth kinetics in the dynamic model.

2.2.1 Comparison of different dynamic models

Two types of dynamic models, the Monod model and the Droop model, are mainly used for microorganism growth simulation. Detailed equations of the Monod model and the Droop model are shown below. The difference between the two models is that the Monod model does not include the accumulation of intracellular nutrient concentration, as it assumes all the intracellular nutrients absorbed by cells are immediately consumed for cell division and maintenance. Hence, the Monod model is not valid in this research because the change of intracellular sulphur concentration needs to be included.

Monod Model

$$\frac{dX}{dt} = r_X X \tag{5a}$$

$$\frac{dS}{dt} = -r_S X \tag{5b}$$

$$r_X = r_{max} \cdot \frac{S}{S + K_S} \tag{5c}$$

$$r_S = Y_{S/X} r_X \tag{5d}$$

where r_X is the cell growth rate, X is the cell density, S is the substrate concentration in the culture, r_S is the consumption rate of substrate, r_{max} is the maximum specific growth rate, K_S is the substrate half velocity coefficient, $Y_{S/X}$ is the substrate yield coefficient.

Droop Model

$$\frac{dX}{dt} = r_X X \tag{6a}$$

$$\frac{dQ}{dt} = r_S - r_X Q \tag{6b}$$

$$\frac{dS}{dt} = -r_S X \tag{6c}$$

$$r_X = r_{max} \cdot f(Q) \tag{6d}$$

$$r_S = Y_{S/X} \cdot r_{max} \cdot \frac{S}{S + K_S} \tag{6e}$$

where Q is the nutrient quota (ratio between intracellular nutrient mass and biomass), $f(Q)$ is the influence of nutrient quota on the microorganism growth rate.

Fouchard et al.[24] has applied the Droop model to simulate green algal growth in a sulphur-deprived culture. Consequently, the values of kinetic parameters presented in his work are selected in the current research. Fouchard et al.[24] also added a cell respiration term in the Droop model as algal respiration rate in this case is quite significant. The modified algal growth equation is shown in Equation (7).

$$\frac{dX}{dt} = r_X X - r_R X \tag{7}$$

where r_{R} is the specific cell respiration rate.

2.2.2 Expression of $f(\mathrm{Q})$ and oxygen net consumption rate

In the Droop model, an accurate expression of $f(\mathrm{Q})$ is essential because it represents the impact of intracellular nutrient concentration on cells growth rate. Specific to the current research, $f(\mathrm{Q})$ represents the influence of intracellular sulphur concentration on photosynthesis activity. Despite its importance, there is no theoretical expression of $f(\mathrm{Q})$ since the influence of intracellular nutrient concentration on cells growth is very complicated. By modifying the expression presented in Fouchard et al.[24], Equation (8) is derived in the current research. Parameters in Equation (8) are fitted using the published experimental data by Melis et al.[4] and shown in Table 2.

$$\frac{f\left(\mathrm{Q}\right)-f_{\min}}{1-f_{\min}}=\left(\frac{\mathrm{Q}}{\mathrm{Q}_{\max}}\right)^{k_{\mathrm{Q}}} \tag{8}$$

where $f_{\min}$ represents the minimum $f(\mathrm{Q})$ corresponding to the minimal intracellular sulphur concentration, $\mathrm{Q}_{\max}$ represents the maximum (saturate) sulphur quota.

The oxygen consumption rate is also important since hydrogenase is activated after the depletion of oxygen. During the operation, oxygen is continuously generated by algal photosynthesis, meanwhile it is consumed by cell respiration. Because of the remarkable damage on PSII, the oxygen production rate drops lower than the oxygen consumption rate and the culture eventually switches to anaerobic condition. Equation (9) is used to calculate oxygen concentration as a function of time. The first term on the right hand side of the equation represents the oxygen production rate, and the second term represents the oxygen consumption rate.

$$\frac{d\mathrm{O}_2}{dt}=0.5\cdot r_{1,L}\cdot\mathrm{X}-Y_{\mathrm{O}_2/\mathrm{X}}\cdot r_{\mathrm{R}}\cdot\mathrm{X} \tag{9}$$

where $r_{1,L}$ is the water-splitting rate, and $Y_{\mathrm{O}_2/\mathrm{X}}$ is the oxygen yield coefficient.

The initial biomass, substrate concentrations, and the kinetic parameters in the current algal growth model can be found in Table 2 and Table 1.

2.3 Sensitivity analysis

Sensitivity analysis is commonly applied to dynamic models to measure the effect of model parameters to model state variables[37,38]. A normalised sensitivity is defined by Equation (10) (Morbidelli and Varma[38]). This normalised sensitivity reflects the proportional change of model output ($z_i(t)$) due to the proportional change of a model parameter (p_j) and in effect comprises an elasticity measure. A positive sensitivity means increasing the parameter can increase the the associated state variable value, whilst a negative sensitivity suggests that increasing the parameter will reduce the associated state variable value. Furthermore, a larger sensitivity also indicates that the effect of the parameter on the model output is greater (more significant).

$$\varepsilon_{ij}(t) = \frac{p_j}{z_i(t)} \cdot \frac{dz_i(t)}{dp_j} \tag{10}$$

In the current study, the state variable studied as model output is hydrogen production and the model parameters are the kinetic constants of the reactions in the metabolic network. As the current work selects Equation (3) to represent the kinetics of metabolic network, the reaction rates are proportional to their kinetic constants. The sensitivity thereby reflects the change of hydrogen production with respect to the change of reaction rate. By conducting extensive sensitivity analysis studies, both the limiting reaction steps and the competing pathways for hydrogen production in the metabolic network are identified.

3 Results and discussion

3.1 Kinetic constants in the model

By using the parameter estimation method proposed in the current research, the kinetic constants in the metabolic reaction network and algal growth model are shown in Table 2.

Table 2: Kinetic parameters in current model. $k_i^\star$ denotes the kinetic constant of reaction i in the anaerobic condition. Since $r_{12,L}$, the hydrogen reduction reaction, does not exist in the aerobic condition, it assumes that HydA has a similar reaction activity compared to FNR (Yacoby et al.[39]). From previous research (Takahashi et al.[10], Alric[35]) it is found that in anaerobic conditions the activity of CEF pathway enhances 3-fold compared to that in aerobic conditions, therefore, $k_{i,C}^\star$ is assumed to be 3-fold of $k_{i,C}$ and not listed in the table. $r_{\max}$ is obtained from (Tamburic et al.[40]); r_{R} is obtained from (Melis et al.[4]); $Y_{\mathrm{O_2/X}}$ is obtained from (Fouchard et al.[24]); $f_{\min}$, k_{Q} and $\mathrm{Q}_{\max}$ are obtained by fitting the data in Melis et al.[4].

Parameter	Value	Unit	Parameter	Value	Unit
$k_{1,L}$	1.08×10^6	$\mathrm{amol \cdot L^{-1} \cdot h^{-1}}$	k_Q	0.596	–
$k_{2,L}$	5.48×10^5	$\mathrm{L \cdot amol^{-1} \cdot h^{-1}}$	$k_{13,L}$	2.16×10^7	$\mathrm{h^{-1}}$
$k_{3,L}$	3.20×10^5	$\mathrm{L \cdot amol^{-1} \cdot h^{-1}}$	$k_{1,C}$	6.85×10^3	$\mathrm{L \cdot amol^{-1} \cdot h^{-1}}$
$k_{4,L}$	1.10×10^7	$\mathrm{L^2 \cdot amol^{-2} \cdot h^{-1}}$	$k_{2,C}$	1.17×10^5	$\mathrm{L \cdot amol^{-1} \cdot h^{-1}}$
$k_{5,L}$	3.20×10^5	$\mathrm{L \cdot amol^{-1} \cdot h^{-1}}$	$k_{3,C}$	6.40×10^4	$\mathrm{L \cdot amol^{-1} \cdot h^{-1}}$
$k_{6,L}$	1.10×10^7	$\mathrm{L^2 \cdot amol^{-2} \cdot h^{-1}}$	$k_{4,C}$	2.19×10^6	$\mathrm{L^2 \cdot amol^{-2} \cdot h^{-1}}$
$k_{7,L}$	1.44×10^6	$\mathrm{h^{-1}}$	$k_{5,C}$	6.40×10^4	$\mathrm{L \cdot amol^{-1} \cdot h^{-1}}$
$k_{8,L}$	1.04×10^5	$\mathrm{L \cdot amol^{-1} \cdot h^{-1}}$	$k_{6,C}$	2.19×10^6	$\mathrm{L^2 \cdot amol^{-2} \cdot h^{-1}}$
$k_{9,L}$	7.83×10^5	$\mathrm{L \cdot amol^{-1} \cdot h^{-1}}$	$k_{7,C}$	2.88×10^5	$\mathrm{h^{-1}}$
$k_{10,L}$	1.50×10^5	$\mathrm{L \cdot amol^{-1} \cdot h^{-1}}$	$k_{8,C}$	2.08×10^4	$\mathrm{L \cdot amol^{-1} \cdot h^{-1}}$
$k_{10,L}^\star$	1.50×10^4	$\mathrm{L \cdot amol^{-1} \cdot h^{-1}}$	$k_{9,C}$	4.32×10^6	$\mathrm{L \cdot amol^{-1} \cdot h^{-1}}$
$k_{11,L}$	9.00×10^5	$\mathrm{h^{-1}}$	$k_{10,C}$	1.57×10^5	$\mathrm{L \cdot amol^{-1} \cdot h^{-1}}$
$k_{12,L}$	0	$\mathrm{h^{-1}}$	$k_{11,C}$	3.00×10^4	$\mathrm{h^{-1}}$
$k_{12,L}^\star$	3.03×10^6	$\mathrm{h^{-1}}$	$r_{\max}$	0.15	$\mathrm{h^{-1}}$
r_{R}	1.08×10^5	$\mathrm{amol \cdot L^{-1} \cdot h^{-1}}$	$Y_{\mathrm{O_2/X}}$	1.42	$\mathrm{mgO_2 \cdot mgX}$
$f_{\min}$	0.056	–	$\mathrm{Q}_{\max}$	9.44	$\mathrm{mgS \cdot mgX}$

3.2 Influence of different metabolic pathways on hydrogen production

The current work compares the simulation results of hydrogen production at different conditions. Figure 4 shows the comparison of simulated hydrogen production when specific pathways are inactivated. From Figure 4, it is found that when all of the pathways in the model are activated, the simulation results of hydrogen production match the experimental results fairly well.

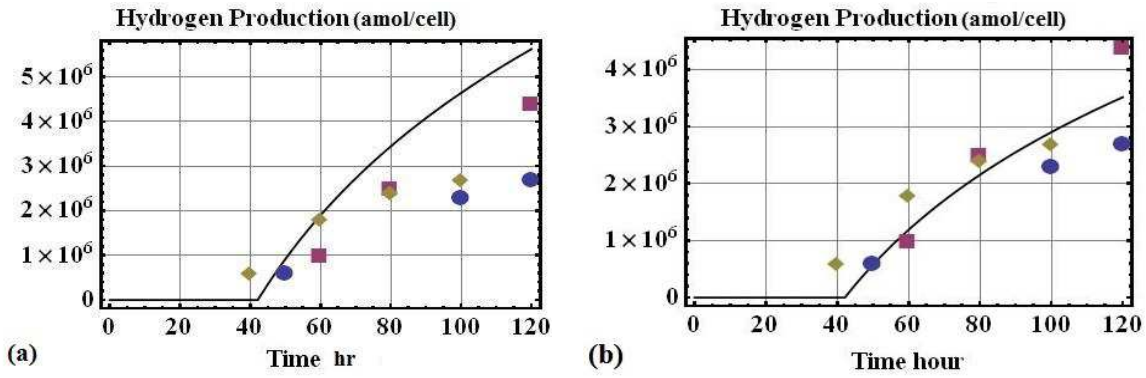

Figure 4: Comparison of hydrogen production at different conditions. (a) only the LEF pathway for hydrogen production is activated; (b) all of the metabolic pathways are activated. Diamond points are measured by Zhang and Melis[9], circle points are measured by Tamburic et al.[40] and square points are measured by Nguyen et al.[41].

Table 3 shows the simulation result of hydrogen production at the 120$^{\text{th}}$ hour of fermentation, when different pathways are activated. It is found that the simulation result only including the hydrogen generation pathway is approximately twice of the experimental result. This is quite similar with previous work[13] which found a 128% increase on hydrogen production by inhibiting the activity of other pathways. By blocking the hydrogen ions transport pathway the current hydrogen production simulation result is significantly enhanced by 25%, which is similar with the 30% increase measured by previous experimental work[13].

A remarkable increase on hydrogen production is also found in the current work by inhibiting the activity of the CEF pathway. However, hydrogen production does not change much when the starch generation pathway is inhibited, suggesting that this pathway is not competitive to the hydrogen generation pathway when the other metabolic pathways are not activated.

Table 3: Comparison of hydrogen production at 120$^{\text{th}}$ hour at different conditions.

Activated metabolic pathways	Hydrogen production
hydrogen production	5.63×10^6 amol×cell^{-1}
hydrogen and starch generation	5.03×10^6 amol×cell^{-1}
Hydrogen and starch pathways and CEF	3.95×10^6 amol×cell^{-1}
All metabolic pathways	3.16×10^6 amol×cell^{-1}
Average experimental result	2.80×10^6 amol×cell^{-1}

Previous research partially explained the reason why the CEF pathway can suppress hydro-

gen production[12,13]. It was claimed that a very high proton gradient from the lumen side to the stroma side of chloroplasts is induced by the enhancement of CEF pathway activity, as the CEF pathway becomes the predominant photosynthetic pathway in anaerobic conditions. The high proton gradient thereby leads to a lack of hydrogen ions at the stroma side. Because the electron transfer chain needs the participation of hydrogen ions at the stroma side, the electron transport rate is sequentially suppressed. Hence, hydrogen production rate is inhibited. The present model also verifies the above conclusion. From the model, it is found that the concentration of hydrogen ions at the stroma side increases from 3-fold to 10-fold compared to that at the lumen side when the CEF pathway is included in the anaerobic condition.

Nevertheless, previous work cannot explain why only a 30% improvement of hydrogen production is observed instead of a 128% improvement when only offsetting the proton gradient rather than inhibiting the activity of the CEF pathway. If the CEF pathway suppresses the hydrogen production pathway solely by inducing a high proton gradient, the increase of hydrogen production by inhibiting the CEF pathway and by offsetting the proton gradient should be the same. Although Antal et al.[13] hypothesised that the CEF pathway also consumes the electrons generated through the water-splitting reaction, which should be used for hydrogen production, this hypothesis is highly doubtful as electrons presented in the CEF pathway are provided by PSI, while those for hydrogen and starch generation are provided by PSII.

As a result, there must be other metabolic pathways consuming the electrons obtained from PSII and suppressing hydrogen production pathway, and CEF pathway should also lower hydrogen production by other mechanisms. This indicates clearly that the pathway is not fully understood and that further research should be conducted to elucidate the matter and complete the existing knowledge about these organisms.

3.3 Influence of different metabolic pathways on starch production

Although the LEF pathway for starch generation is the major algal photosynthetic pathway

in aerobic conditions, few researchers have focused on the study of this pathway during the hydrogen production period. Previous research[42] mentions that this pathway may exist in anaerobic conditions, but its activity is supposed to be severely inhibited and not competitive to the hydrogen production pathway. To verify that starch is generated during the hydrogen production period, the current work simulates the consumption rate of starch under different conditions.

Figure 5 compares the net accumulation of intracellular starch concentration in a sulphur deprived culture with the absence or presence of starch generation pathway. The initial increasing period happens when the culture is still aerobic, and it is followed by the consumption period after the culture switches to anaerobic. Since the current work assumes that all the electrons from photosynthesis during aerobic conditions are used for starch generation, the initial accumulation of starch is decidedly overestimated. However, this overestimation does not have much effect on the current work, as it is mainly focused on the simulation of the anaerobic period.

From Figure 5, it is found that the starch consumption rate which excludes the starch generation pathway in the anaerobic condition is much sharper than previous experimental results, whilst that including the starch generation pathway shows very similar tendency compared to the experimental results as the deviation between the simulation and experimental results is almost constant. Therefore the current simulation results conclusively indicate that the starch generation pathway still exists in the anaerobic condition.

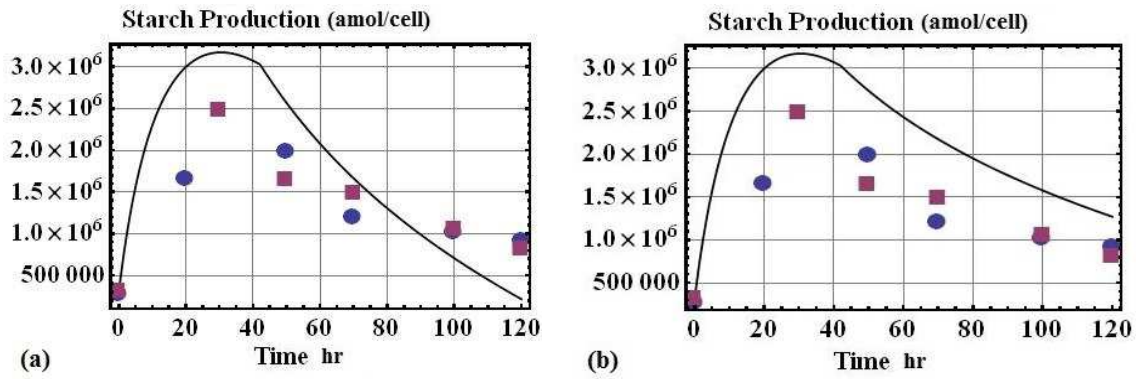

Figure 5: Comparison of net accumulation of intracellular starch at different conditions. (a) starch generation pathway is not included in the anaerobic condition; (b) starch generation pathway is included in the anaerobic condition. Square points are reported by Tolleter et al.[12], and the circle points are reported by Chochois et al.[28].

Previous research[43] also found that when the Calvin-Benson cycle (the important pathway for starch generation) is destroyed in an algal mutant, whose photosynthetic activity is much lower than the wild type, more hydrogen can be generated than before. For the wild type algae, a slight increase on hydrogen production is also observed even if the experiment is stopped in the initial hydrogen production period[43]. Both experimental observations indicate that there is a significant competition between the starch generation pathway and the hydrogen generation pathway.

Despite the current work having demonstrated that the starch generation pathway is not competitive with the hydrogen generation pathway if other pathways are inactivated, attention has to be paid to the fact that many other metabolic pathways are actually activated. In particular, the CEF pathway and the starch generation pathway share the same metabolic reaction which is the electron transfer step catalysed by FNR from ferredoxin to $NAD(P)^+$. When the CEF pathway does not exist, electrons from ferredoxin may mainly be sent to hydrogenase for hydrogen reduction as the activity of starch generation pathway is severely damaged in the anaerobic condition. Nevertheless, because the CEF pathway is the major photosynthetic pathway in the anaerobic condition, it is quite possible that electrons from ferredoxin are mainly sent to $NAD(P)^+$ to cycle through the CEF pathway. Since the

CEF pathway only utilities the electrons provided by PSI, the electrons generated by PSII but accepted by $NAD(P)^+$ through the CEF pathway will be sent to the starch generation pathway. Thus the activity of the starch generation pathway can be partially recovered.

Based on the current modelling results, two hypotheses are proposed in this work: 1. the starch generation pathway mainly competes with the hydrogen production pathway, and limits the hydrogen production rate; 2. the CEF pathway suppresses hydrogen production not only by inducing a high proton gradient, but also by enhancing the activity of starch generation pathway.

3.4 Identification of limiting steps and competing metabolic pathways

To verify the hypotheses proposed in current research, sensitivity analysis is conducted in the current model.

The sensitivity of hydrogen production with respect to different reaction rates are shown in Figure 6. Figure 6(a) shows the positive sensitivities, which implies that these reactions are the limiting reaction steps for hydrogen production in the hydrogen generation pathway. By improving the reaction rates of these reactions, hydrogen production can be enhanced. For example, it can be found that a 1% increase on the reaction rate of r_{12} (the reduction of hydrogen ions catalysed by hydrogenase) can lead to a 0.5% increase on hydrogen production independently of fermentation time. The water-splitting reaction is found to have the highest sensitivity, although its value slightly decreases with operating time, which means it is the major limiting reaction step for hydrogen production.

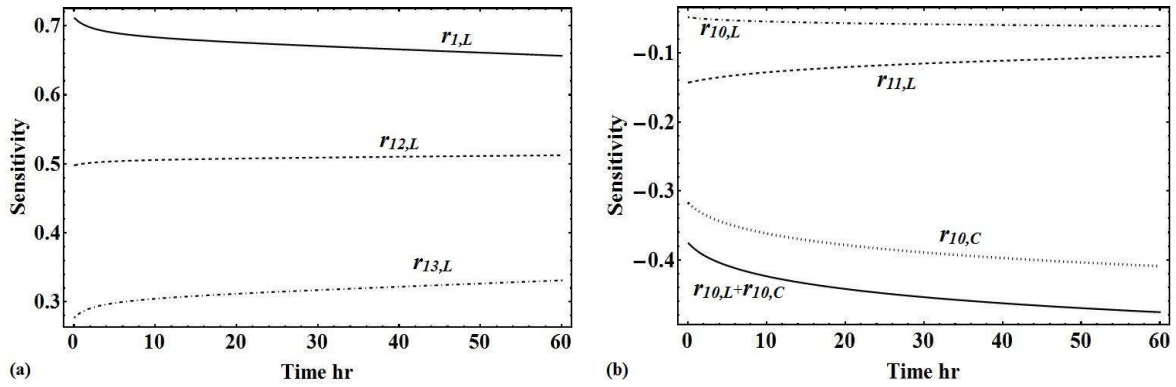

Figure 6: Sensitivity of hydrogen production w.r.t. the reaction rate of different reactions. (a) positive sensitivity. The solid line represents reaction 1 ($r_{1,L}$), the water-splitting. The dashed line denotes reaction 12 ($r_{12,L}$), the hydrogen ions reduction by hydrogenase. The dot-dashed line represents reaction 13 ($r_{13,L}$), the transport of hydrogen ions from lumen side to stroma side. (b) negative sensitivity. The solid line represents the FNR catalysed reaction (electrons transfer between Fd and $NAD(P)^+$) in both starch generation and CEF pathways ($r_{10,L} + r_{10,C}$). The dashed line denotes the starch generation reaction ($r_{11,L}$, a simplified reaction to represent the Calvin-Benson cycle). The dot-dashed line represents the FNR catalysed reaction only in the starch generation pathway ($r_{10,L}$). The dotted line denotes the FNR catalysed reaction only in CEF pathway ($r_{10,C}$).

Figure 6(b) presents the negative sensitivities, and suggests that these reactions are the competing metabolic pathways for hydrogen production. By inhibiting the activity of these reactions, hydrogen production will be improved. It is easy to see that the FNR catalysed reaction (the electron transfer step from Fd to $NAD(P)^+$) only shows negligible influence on hydrogen production if the CEF pathway is not included. However, its effect is markedly enhanced by the presence of the CEF pathway, and becomes the major competing reaction step (the same reaction step exists in both starch generation pathway and CEF pathway, $r_{10,L} + r_{10,C}$) for hydrogen production. As a result, more electrons are transported to the starch generation pathway because of the high activity of the CEF pathway, and the current hypotheses are verified.

Table 4: The rank of the sensitivity of hydrogen production w.r.t. different reaction steps in the current metabolic network.

	0^{th} hr	10^{th} hr	50^{th} hr
1	$r_{1,L}$ (+0.711)	$r_{1,L}$ (+0.683)	$r_{1,L}$ (+0.659)
2	$r_{12,L}$ (+0.499)	$r_{12,L}$ (+0.506)	$r_{12,L}$ (+0.511)
3	$r_{10,L} + r_{10,C}$ (-0.379)	$r_{10,L} + r_{10,C}$ (-0.425)	$r_{10,L} + r_{10,C}$ (-0.471)
4	$r_{10,C}$ (-0.319)	$r_{10,C}$ (-0.361)	$r_{10,C}$ (-0.405)
5	$r_{13,L}$ (+0.263)	$r_{13,L}$ (+0.304)	$r_{13,L}$ (+0.326)
6	$r_{11,L}$ (-0.143)	$r_{11,L}$ (-0.126)	$r_{11,L}$ (-0.108)
7	$r_{10,L}$ (-0.049)	$r_{10,L}$ (-0.053)	$r_{10,L}$ (-0.059)

To optimise hydrogen production, it is very important to ensure that the fermentation process is conducted in operating conditions such that the most sensitive reaction steps do not limit hydrogen production. Since sensitivity reflects the importance of reaction steps on hydrogen production (over the course of time), by ranking sensitivities the significance of each reaction step on hydrogen production can be obtained.

From Table 4 it is seen that the order of the reactions with the highest sensitivity measure does not change with time, and algal hydrogen production is primarily limited by the activity of the hydrogen generation pathway instead of the competing pathways. It is noted that other reactions have much less sensitivity compared to those represented in the table, which indicates their unimportant influence on hydrogen production. Therefore they are not shown in Table 4.

Therefore, compared to considerations to add chemicals to inhibit the activity of competing pathways, or to develop new mutants with a low activity of the starch generation pathway, it is more important to focus on enhancing the activity of $r_{1,L}$ (water-splitting step). Since the activity of $r_{1,L}$ is predominantly affected by the intracellular sulphur concentration, the optimal reactor type (fed-batch, batch, or continuous reactor) and the associated optimal sulphur concentration in the culture should be determined by further work.

Previous research suggests that the diffusion of small proteins such as PQ and PC may limit the overall reaction rate of the electron transfer chain, and then suppresses the hydrogen production rate[29,44]. As the current parameter estimation method can only calculate the

apparent kinetic constant which corresponds to the apparent reaction rate, the present model is not capable of detecting if these reactions are lowered by the diffusion of small proteins. However, the current study finds that the sensitivity of hydrogen production with respect to the reactions potentially including the diffusion of small proteins is negligible, which means hydrogen production is almost independent of the apparent activity of these reactions. Hence even if the diffusion of small proteins does exist, it should not suppress hydrogen production.

3.5 Impact of the initial concentration of proteins on hydrogen production

Finally, to check if the concentration of different types of proteins under different states (oxidised or reduced) has significant impact on the simulated hydrogen production, sensitivity analysis is also used to measure this effect. It is found that hydrogen production is most sensitive to the initial concentration of NAD(P) and $NAD(P)^+$(both of them have a sensitivity of -0.26), and also PQ (a sensitivity of 0.18).

In terms of other proteins, it is found that hydrogen production is slightly affected by two kinds of large protein complex ($[fb \cdot PQH]^+$ and $[fb \cdot PQ]^+$), as their sensitivities are 0.019. The sensitivity to the initial concentration of other proteins is much lower than 0.019 and can be neglected.

A more accurate concentration of NAD(P), $NAD(P)^+$ and PQ should be measured in the future to improve the accuracy of the current model. It is also important to note that the accuracy of the current model is not much influenced by the initial concentration of any proteins, since the greatest sensitivity is only -0.26. Hence the current simplification that the different states of each protein have the same initial intracellular concentration is acceptable.

4 Conclusion

Because of the unsteady-state (dynamic) fermentation processes, the current study proposes a methodology for dynamic model construction to determine the limiting nature of key steps

and competing metabolic pathways in biochemical processes. The methodology is applied to green algae hydrogen production. A novel parameter estimation method is proposed to facilitate the construction of the current model.

By blocking the activity of specific pathways and comparing with the previous experimental results, the accuracy of the proposed model is verified. The present work proposes that the starch generation pathway mainly competes with the hydrogen production pathway, since its activity is remarkably enhanced by the cyclic electron flow pathway.

By carrying out a dynamic sensitivity analysis, the current work suggests different solutions to improve hydrogen production. It is also concluded that the water-splitting step is the primary reaction limiting hydrogen production. As the reaction rate of water-splitting is determined by the activity of photosystem II which is dependent on the intracellular sulphur concentration, further work should try to find the optimal sulphur concentration in the culture so that the activity of photosystem II can be kept high and the culture can be maintained in the anaerobic condition.

Acknowledgments

Author D. Zhang gratefully acknowledges the support from his family. The authors would also like to acknowledge Mr. Fabio Fiorelli for his meaningful suggestions. Finally, the authors wish to thank the anonymous referees for their insightful comments.

References

(1) Kumar, K.; Dasgupta, C.; Nayak, B. Development of suitable photobioreactors for CO2 sequestration addressing global warming using green algae and cyanobacteria. *Bioresource technology* **2011**, *102*, 4945–53.

(2) Yildiz, B.; Conzelmann, G.; Petri, M. C.; Forsberg, C.

(3) Pott, R. W. M.; Howe, C. J.; Dennis, J. S. Photofermentation of crude glycerol from biodiesel using Rhodopseudomonas palustris: comparison with organic acids and the identification of inhibitory compounds. *Bioresource technology* **2013**, *130*, 725–730.

(4) Melis, A.; Zhang, L.; Forestier, M. Sustained photobiological hydrogen gas production upon reversible inactivation of oxygen evolution in the green alga Chlamydomonas reinhardtii. *Plant physiology* **2000**, *122*, 127–36.

(5) Catalanotti, C.; Yang, W.; Posewitz, M. Fermentation metabolism and its evolution in algae. *Frontiers in plant science* **2013**, *4*, 150.

(6) Mus, F.; Dubini, A.; Seibert, M. Anaerobic acclimation in Chlamydomonas reinhardtii: anoxic gene expression, hydrogenase induction, and metabolic pathways. *The Journal of biological chemistry* **2007**, *282*, 25475–86.

(7) Antal, T.; Krendeleva, T.; Rubin, A. Acclimation of green algae to sulfur deficiency: underlying mechanisms and application for hydrogen production. *Applied microbiology and biotechnology* **2011**, *89*, 3–15.

(8) Ghysels, B.; Franck, F. Hydrogen photo-evolution upon S deprivation stepwise: an illustration of microalgal photosynthetic and metabolic flexibility and a step stone for future biotechnological methods of renewable H2 production. *Photosynthesis research* **2010**, *106*, 145–54.

(9) Zhang, L.; Melis, A. Probing green algal hydrogen production. *Philosophical transactions of the Royal Society of London. Series B, Biological sciences* **2002**, *357*, 1499–507; discussion 1507–11.

(10) Takahashi, H.; Clowez, S.; Wollman, F. Cyclic electron flow is redox-controlled but independent of state transition. *Nature communications* **2013**, *4*, 1954–1962.

(11) Iwai, M.; Takizawa, K.; Tokutsu, R. Isolation of the elusive supercomplex that drives cyclic electron flow in photosynthesis. *Nature* **2010**, *464*, 1210–3.

(12) Tolleter, D.; Ghysels, B.; Alric, J. Control of hydrogen photoproduction by the proton gradient generated by cyclic electron flow in Chlamydomonas reinhardtii. *The Plant cell* **2011**, *23*, 2619–30.

(13) Antal, T.; Volgusheva, A.; Kukarskih, G. Relationships between H2 photoproduction and different electron transport pathways in sulfur-deprived Chlamydomonas reinhardtii. *International Journal of Hydrogen Energy* **2009**, *34*, 9087–9094.

(14) Fischer, N.; Sétif, P.; Rochaix, J. Targeted mutations in the psaC gene of Chlamydomonas reinhardtii: preferential reduction of FB at low temperature is not accompanied by altered electron flow from photosystem I to ferredoxin. *Biochemistry* **1997**, *36*, 93–102.

(15) Hippler, M.; Drepper, F.; Farah, J. Fast electron transfer from cytochrome c6 and plastocyanin to photosystem I of Chlamydomonas reinhardtii requires PsaF. *Biochemistry* **1997**, *36*, 6343–9.

(16) Chow, W.; Hope, A. Kinetics of reactions around the cytochrome bf complex studied in intact leaf disks. *Photosynthesis research* **2004**, *81*, 153–163.

(17) Winkler, M.; Kuhlgert, S.; Hippler, M. Characterization of the key step for light-driven hydrogen evolution in green algae. *The Journal of biological chemistry* **2009**, *284*, 36620–7.

(18) White, A.; Melis, A. Biochemistry of hydrogen metabolism in Chlamydomonas reinhardtii wild type and a Rubisco-less mutant. *International Journal of Hydrogen Energy* **2006**, *31*, 455–464.

(19) Dal'Molin, C.; Quek, L.; Palfreyman, R. AlgaGEM–a genome-scale metabolic reconstruction of algae based on the Chlamydomonas reinhardtii genome. *BMC genomics* **2011**, *12 Suppl 4*, S5.

(20) Pan, P.; Hua, Q. Reconstruction and in silico analysis of metabolic network for an oleaginous yeast, Yarrowia lipolytica. *PloS one* **2012**, *7*, 51535–51546.

(21) McKinlay, J. B.; Oda, Y.; Rühl, M.; Posto, A. L.; Sauer, U.; Harwood, C. S. Nongrowing Rhodopseudomonas palustris increases the hydrogen gas yield from acetate by shifting from the glyoxylate shunt to the tricarboxylic acid cycle. *The Journal of biological chemistry* **2014**, *289*, 1960–70.

(22) McKinlay, J. B.; Harwood, C. S. Calvin Cycle Flux , Pathway Constraints , and Substrate Oxidation State Together Determine the H2 Biofuel Yield in Photoheterotrophic Bacteria. *mBio* **2011**, *2*, 1–9.

(23) Pai, T.-y.; Lai, W.-j. Analyzing Algae Growth and Oil Production in a Batch Reactor under high Nitrogen and Phosphorus Conditions. *International Journal of Applied Science and Engineering* **2011**, *9*, 161–168.

(24) Fouchard, S.; Pruvost, J.; Degrenne, B. Kinetic modeling of light limitation and sulfur deprivation effects in the induction of hydrogen production with Chlamydomonas reinhardtii: Part I. Model development and parameter identification. *Biotechnology and bioengineering* **2009**, *102*, 232–45.

(25) Alwan, G. Simulation and Optimization of a Continuous Biochemical Reactor. *Journal of Chemical Engineering & Process Technology* **2012**, *04*, 1–7.

(26) Degrenne, B.; Pruvost, J.; Titica, M.; Takache, H.; Legrand, J. Kinetic modeling of light limitation and sulfur deprivation effects in the induction of hydrogen production with Chlamydomonas reinhardtii. Part II: Definition of model-based protocols and experimental validation. *Biotechnology and bioengineering* **2011**, *108*, 2288–2299.

(27) Klipp, E.; Herwig, R.; Kowald, A. *Systems biology in practice*; WILEY-VCH Verlag GmbH & Co. KGaA: Weinheim, 2005; p 463.

(28) Chochois, V.; Dauvillée, D.; Beyly, A.; Tolleter, D.; Cuiné, S.; Timpano, H.; Ball, S.; Cournac, L.; Peltier, G. Hydrogen production in Chlamydomonas: photosystem II-dependent and -independent pathways differ in their requirement for starch metabolism. *Plant physiology* **2009**, *151*, 631–40.

(29) Hope, a. B. Electron transfers amongst cytochrome f, plastocyanin and photosystem I: kinetics and mechanisms. *Biochimica et biophysica acta* **2000**, *1456*, 5–26.

(30) Forti, G.; Furia, A.; Bombelli, P.; Finazzi, G.; Nazionale, C.; Milano, S.; Biologia, D.; Celoria, V. In Vivo Changes of the Oxidation-Reduction State of NADP and of the ATP / ADP Cellular Ratio Linked to the Photosynthetic Activity in Chlamydomonas reinhardtii. *Plant physiology* **2003**, *132*, 1464–1474.

(31) Reubelt, U.; Wohlfarth, G.; Sehmid, R.; Diekert, G. Purification and characterization of ferredoxin from Peptostreptococcus productus (strain Marburg). *Archives of Microbiology* **1991**, *156*, 422–426.

(32) Bonente, G.; Pippa, S.; Castellano, S.; Bassi, R.; Ballottari, M. Acclimation of Chlamydomonas reinhardtii to different growth irradiances. *The Journal of biological chemistry* **2012**, *287*, 5833–47.

(33) Kirst, H.; Garcia-Cerdan, J. G.; Zurbriggen, A.; Ruehle, T.; Melis, A. Truncated photosystem chlorophyll antenna size in the green microalga Chlamydomonas reinhardtii upon deletion of the TLA3-CpSRP43 gene. *Plant physiology* **2012**, *160*, 2251–60.

(34) Melis, A.; Eroglu, E. Extraction of extracellular terpenoids from microalgae colonies. 2011.

(35) Alric, J. Cyclic electron flow around photosystem I in unicellular green algae. *Photosynthesis research* **2010**, *106*, 47–56.

(36) Schomburg, I.; Chang, A.; Placzek, S.; Söhngen, C.; Rother, M.; Lang, M.; Munaretto, C.; Ulas, S.; Stelzer, M.; Grote, A.; Scheer, M.; Schomburg, D. BRENDA in 2013: integrated reactions, kinetic data, enzyme function data, improved disease classification: new options and contents in BRENDA. *Nucleic acids research* **2013**, *41*, D764–72.

(37) Klipp, E.; Herwig, R.; Kowald, A.; Wierling, C.; Lehrach, H. *Systems biology in practice: Concepts, implementation and application.*; WILEY-VCH Verlag GmbH & Co. KGaA: Weinheim, 2005.

(38) Morbidelli, M.; Varma, A. A generalized criterion for parametric sensitivity: application to thermal explosion theory. *Chemical Engineering Science* **1988**, *43*, 91–102.

(39) Yacoby, I.; Pochekailov, S.; Toporik, H.; Ghirardi, M. L.; King, P. W.; Zhang, S. Photosynthetic electron partitioning between [FeFe]-hydrogenase and ferredoxin:NADP+-oxidoreductase (FNR) enzymes in vitro. *Proceedings of the National Academy of Sciences of the United States of America* **2011**, *108*, 9396–401.

(40) Tamburic, B.; Zemichael, F. W.; Maitland, G. C.; Hellgardt, K. A novel nutrient control method to deprive green algae of sulphur and initiate spontaneous hydrogen production. *International Journal of Hydrogen Energy* **2012**, *37*, 8988–9001.

(41) Nguyen, A.; Toepel, J.; Burgess, S. Time-course global expression profiles of Chlamydomonas reinhardtii during photo-biological Hydrogen production. *PloS one* **2011**, *6*, e29364.

(42) Hemschemeier, A. The anaerobic life of the photosynthetic alga Chlamydomonas reinhardtii Photofermentation and hydrogen production upon Das anaerobe Leben der photosynthetischen Alge Chlamydomonas reinhardtii. Ph.D. thesis, 2005.

(43) Rühle, T.; Hemschemeier, A.; Melis, A.; Happe, T. A novel screening protocol for the isolation of hydrogen producing Chlamydomonas reinhardtii strains. *BMC plant biology* **2008**, *8*, 107–120.

(44) Mamedov, F. Personal Communication. 2014.

Appendix

1 Metabolic reaction network

Linear electron flow

water-splitting reaction, $r_{1,L}$

$$\mathrm{PQ} + \mathrm{H_2O} \longrightarrow \mathrm{PQH_2} + \tfrac{1}{2}\,\mathrm{O_2} \tag{11a}$$

$[\mathrm{fb}\cdot\mathrm{PQ}]$ generation reaction, $r_{2,L}$

$$\mathrm{PQ} + \mathrm{fb} \longrightarrow [\mathrm{fb}\cdot\mathrm{PQ}] \tag{11b}$$

Pc^+ reduction reaction, $r_{3,L}$

$$[\mathrm{fb}\cdot\mathrm{PQ}] + \mathrm{Pc}^+ \longrightarrow \mathrm{Pc} + [\mathrm{fb}\cdot\mathrm{PQ}]^+ \tag{11c}$$

$\mathrm{PQH_2}$ oxidation reaction, $r_{4,L}$

$$[\mathrm{fb}\cdot\mathrm{PQ}]^+ + \mathrm{PQH_2} + {\mathrm{H_S}}^+ \longrightarrow \mathrm{PQ} + [\mathrm{fb}\cdot\mathrm{PQH}] + 2\,{\mathrm{H_L}}^+ \tag{11d}$$

Pc^+ reduction reaction, $r_{5,L}$

$$[\mathrm{fb}\cdot\mathrm{PQH}] + \mathrm{Pc}^+ \longrightarrow \mathrm{Pc} + [\mathrm{fb}\cdot\mathrm{PQH}]^+ \tag{11e}$$

PQH_2 oxidation reaction, $r_{6,L}$

$$[\mathrm{fb}\cdot\mathrm{PQH}]^+ + \mathrm{PQH_2} + {\mathrm{H_S}}^+ \longrightarrow \mathrm{PQ} + [\mathrm{fb}\cdot\mathrm{PQH_2}] + 2\,{\mathrm{H_L}}^+ \tag{11f}$$

$[\mathrm{fb}\cdot\mathrm{PQH_2}]$ decomposition reaction, $r_{7,L}$

$$[\mathrm{fb}\cdot\mathrm{PQH_2}] \longrightarrow \mathrm{fb} + \mathrm{PQH_2} \tag{11g}$$

PSI^+ reduction reaction, $r_{8,L}$

$$2\,\mathrm{PSI}^+ + 2\,\mathrm{Pc} \longrightarrow 2\,\mathrm{Pc}^+ + 2\,\mathrm{PSI} \tag{11h}$$

Fd^+ reduction reaction, $r_{9,L}$

$$2\,\mathrm{Fd}^+ + 2\,\mathrm{PSI} \longrightarrow 2\,\mathrm{PSI}^+ + 2\,\mathrm{Fd} \tag{11i}$$

NADP^+ reduction reaction, $r_{10,L}$

$$\mathrm{NADP}^+ + 2\,\mathrm{Fd} + \mathrm{H}^+ \longrightarrow 2\,\mathrm{Fd}^+ + \mathrm{NADPH} \tag{11j}$$

$[\mathrm{CH_2O}]$ generation reaction, $r_{11,L}$

$$\mathrm{NADPH} + \tfrac{1}{2}\,\mathrm{CO_2} + \mathrm{H}^+ \longrightarrow \tfrac{1}{2}\,[\mathrm{CH_2O}] + \tfrac{1}{2}\,\mathrm{H_2O} + \mathrm{NADP}^+ \tag{11k}$$

$\mathrm{H_2}$ generation reaction, $r_{12,L}$

$$2\,\mathrm{Fd} + 2\,\mathrm{H}^+ \longrightarrow 2\,\mathrm{Fd}^+ + \mathrm{H_2} \tag{11l}$$

${\mathrm{H_L}}^+$ transport reaction, $r_{13,L}$

$$\mathrm{ADP}^{3-} + \mathrm{Pi}^{2-} + 3\,{\mathrm{H_L}}^+ + {\mathrm{H_S}}^+ \longrightarrow \mathrm{ATP}^{4-} + \mathrm{H_2O} + 3\,{\mathrm{H_S}}^+ \tag{11m}$$

Cyclic electron flow

$\underline{\mathrm{PQH_2}\text{ generation reaction, } r_{1,C}}$

$$\mathrm{PQ} + \mathrm{NADPH} + \mathrm{H^+} \longrightarrow \mathrm{PQH_2} + \mathrm{NADP^+} \tag{12a}$$

$\underline{[\mathrm{fb} \cdot \mathrm{PQ}]\text{ generation reaction, } r_{2,C}}$

$$\mathrm{PQ} + \mathrm{fb} \longrightarrow [\mathrm{fb} \cdot \mathrm{PQ}] \tag{12b}$$

$\underline{\mathrm{Pc^+}\text{ reduction reaction, } r_{3,C}}$

$$[\mathrm{fb} \cdot \mathrm{PQ}] + \mathrm{Pc^+} \longrightarrow \mathrm{Pc} + [\mathrm{fb} \cdot \mathrm{PQ}]^+ \tag{12c}$$

$\underline{\mathrm{PQH_2}\text{ oxidation reaction, } r_{4,C}}$

$$[\mathrm{fb} \cdot \mathrm{PQ}]^+ + \mathrm{PQH_2} + \mathrm{H_S}^+ \longrightarrow \mathrm{PQ} + [\mathrm{fb} \cdot \mathrm{PQH}] + 2\,\mathrm{H_L}^+ \tag{12d}$$

$\underline{\mathrm{Pc^+}\text{ reduction reaction, } r_{5,C}}$

$$[\mathrm{fb} \cdot \mathrm{PQH}] + \mathrm{Pc^+} \longrightarrow \mathrm{Pc} + [\mathrm{fb} \cdot \mathrm{PQH}]^+ \tag{12e}$$

$\underline{\mathrm{PQH_2}\text{ oxidation reaction, } r_{6,C}}$

$$[\mathrm{fb} \cdot \mathrm{PQH}]^+ + \mathrm{PQH_2} + \mathrm{H_S}^+ \longrightarrow \mathrm{PQ} + [\mathrm{fb} \cdot \mathrm{PQH_2}] + 2\,\mathrm{H_L}^+ \tag{12f}$$

$\underline{[\mathrm{fb} \cdot \mathrm{PQH_2}]\text{ decomposition reaction, } r_{7,C}}$

$$[\mathrm{fb} \cdot \mathrm{PQH_2}] \longrightarrow \mathrm{fb} + \mathrm{PQH_2} \tag{12g}$$

$\underline{\mathrm{PSI^+}\text{ reduction reaction, } r_{8,C}}$

$$2\,\mathrm{PSI}^{+} + 2\,\mathrm{Pc} \longrightarrow 2\,\mathrm{Pc}^{+} + 2\,\mathrm{PSI} \tag{12h}$$

Fd^{+} reduction reaction, $r_{9,C}$

$$2\,\mathrm{Fd}^{+} + 2\,\mathrm{PSI} \longrightarrow 2\,\mathrm{PSI}^{+} + 2\,\mathrm{Fd} \tag{12i}$$

NADP^{+} reduction reaction, $r_{10,C}$

$$\mathrm{NADP}^{+} + 2\,\mathrm{Fd} + \mathrm{H}^{+} \longrightarrow 2\,\mathrm{Fd}^{+} + \mathrm{NADPH} \tag{12j}$$

$\mathrm{H_L}^{+}$ transport reaction, $r_{11,C}$

$$\mathrm{ADP}^{3-} + \mathrm{Pi}^{2-} + 3\,\mathrm{H_L}^{+} + \mathrm{H_S}^{+} \longrightarrow \mathrm{ATP}^{4-} + \mathrm{H_2O} + 3\,\mathrm{H_S}^{+} \tag{12k}$$

Reactions in the hydrogen ion transport pathway are included in the LEF and CEF pathways for convenience.

2 Kinetic equations

Linear electron flow

water-splitting reaction

$$r_{1,L} = k_{1,L} \cdot f\,(\mathrm{Q})^{1.5} \tag{13a}$$

$[\mathrm{fb} \cdot \mathrm{PQ}]$ generation reaction

$$r_{2,L} = k_{2,L} \cdot \mathrm{fb} \cdot \mathrm{PQ} \tag{13b}$$

Pc^{+} reduction reaction

$$r_{3,L} = k_{3,L} \cdot [\mathrm{fb} \cdot \mathrm{PQ}] \cdot \mathrm{Pc}^{+} \tag{13c}$$

$\mathrm{PQH_2}$ oxidation reaction

$$r_{4,L} = k_{4,L} \cdot [\mathrm{fb} \cdot \mathrm{PQ}]^{+} \cdot \mathrm{PQH_2} \cdot {\mathrm{H_S}}^{+} \tag{13d}$$

Pc^{+} reduction reaction

$$r_{5,L} = k_{5,L} \cdot [\mathrm{fb} \cdot \mathrm{PQH}] \cdot \mathrm{Pc}^{+} \tag{13e}$$

$\mathrm{PQH_2}$ oxidation reaction

$$r_{6,L} = k_{6,L} \cdot [\mathrm{fb} \cdot \mathrm{PQH}]^{+} \cdot \mathrm{PQH_2} \cdot {\mathrm{H_S}}^{+} \tag{13f}$$

$[\mathrm{fb} \cdot \mathrm{PQH_2}]$ decomposition reaction

$$r_{7,L} = k_{7,L} \cdot [\mathrm{fb} \cdot \mathrm{PQH_2}] \tag{13g}$$

PSI^{+} reduction reaction

$$r_{8,L} = k_{8,L} \cdot \mathrm{PSI}^{+} \cdot \mathrm{Pc} \tag{13h}$$

Fd^{+} reduction reaction

$$r_{9,L} = k_{9,L} \cdot \mathrm{PSI} \cdot \mathrm{Fd}^{+} \tag{13i}$$

NADP^{+} reduction reaction

$$r_{10,L} = k_{10,L} \cdot \mathrm{Fd} \cdot \mathrm{NADP}^{+} \tag{13j}$$

$[\mathrm{CH_2O}]$ generation reaction

$$r_{11,L} = k_{11,L} \cdot \mathrm{NADPH} \tag{13k}$$

H_2 generation reaction

$$r_{12,L} = k_{12,L} \cdot \mathrm{Fd} \tag{13l}$$

$H_L{}^+$ transport reaction

$$r_{13,L} = k_{13,L} \cdot {H_L}^+ \cdot f(\mathrm{Q})^{1.5} \tag{13m}$$

Cyclic electron flow

PQH_2 generation reaction

$$r_{1,C} = k_{1,C} \cdot \mathrm{PQ} \cdot \mathrm{NADPH} \tag{14a}$$

$[\mathrm{fb} \cdot \mathrm{PQ}]$ generation reaction

$$r_{2,C} = k_{2,C} \cdot \mathrm{fb} \cdot \mathrm{PQ} \tag{14b}$$

Pc^+ reduction reaction

$$r_{3,C} = k_{3,C} \cdot [\mathrm{fb} \cdot \mathrm{PQ}] \cdot \mathrm{Pc}^+ \tag{14c}$$

PQH_2 oxidation reaction

$$r_{4,C} = k_{4,C} \cdot [\mathrm{fb} \cdot \mathrm{PQ}]^+ \cdot \mathrm{PQH_2} \cdot {H_S}^+ \tag{14d}$$

Pc^+ reduction reaction

$$r_{5,C} = k_{5,C} \cdot [\mathrm{fb} \cdot \mathrm{PQH}] \cdot \mathrm{Pc}^{+} \tag{14e}$$

$\underline{\mathrm{PQH_2 \text{ oxidation reaction}}}$

$$r_{6,C} = k_{6,C} \cdot [\mathrm{fb} \cdot \mathrm{PQH}]^{+} \cdot \mathrm{PQH_2} \cdot \mathrm{H_S}^{+} \tag{14f}$$

$\underline{[\mathrm{fb} \cdot \mathrm{PQH_2}] \text{ decomposition reaction}}$

$$r_{7,C} = k_{7,C} \cdot [\mathrm{fb} \cdot \mathrm{PQH_2}] \tag{14g}$$

$\underline{\mathrm{PSI}^{+} \text{ reduction reaction}}$

$$r_{8,C} = k_{8,C} \cdot \mathrm{PSI}^{+} \cdot \mathrm{Pc} \tag{14h}$$

$\underline{\mathrm{Fd}^{+} \text{ reduction reaction}}$

$$r_{9,C} = k_{9,C} \cdot \mathrm{PSI} \cdot \mathrm{Fd}^{+} \tag{14i}$$

$\underline{\mathrm{NADP}^{+} \text{ reduction reaction}}$

$$r_{10,C} = k_{10,C} \cdot \mathrm{Fd} \cdot \mathrm{NADP}^{+} \tag{14j}$$

$\underline{\mathrm{H_L}^{+} \text{ transport reaction}}$

$$r_{11,C} = k_{11,C} \cdot \mathrm{H_L}^{+} \cdot f(\mathrm{Q})^{1.5} \tag{14k}$$

3 Mass balance equations

$$\frac{d\,(\mathrm{PQ})}{dt} = -r_{1,L} - r_{2,L} + r_{4,L} + r_{6,L} - r_{2,C} - r_{1,C} + r_{4,C} + r_{6,C} \tag{15a}$$

$$\frac{d\left(\mathrm{PQH_2}\right)}{dt} = -r_{4,L} - r_{6,L} + r_{1,L} + r_{7,L} + r_{1,C} - r_{4,C} - r_{6,C} + r_{7,C} \tag{15b}$$

$$\frac{d\left(\mathrm{fb}\right)}{dt} = -r_{2,L} + r_{7,L} - r_{2,C} + r_{7,C} \tag{15c}$$

$$\frac{d\left(\left[\mathrm{fb}\cdot\mathrm{PQH_2}\right]\right)}{dt} = r_{6,L} - r_{7,L} + r_{6,C} - r_{7,C} \tag{15d}$$

$$\frac{d\left(\left[\mathrm{fb}\cdot\mathrm{PQ}\right]\right)}{dt} = r_{2,L} - r_{3,L} + r_{2,C} - r_{3,C} \tag{15e}$$

$$\frac{d\left(\left[\mathrm{fb}\cdot\mathrm{PQ}\right]^{+}\right)}{dt} = r_{3,L} - r_{4,L} + r_{3,C} - r_{4,C} \tag{15f}$$

$$\frac{d\left(\left[\mathrm{fb}\cdot\mathrm{PQH}\right]\right)}{dt} = r_{4,L} - r_{5,L} + r_{4,C} - r_{5,C} \tag{15g}$$

$$\frac{d\left(\left[\mathrm{fb}\cdot\mathrm{PQH}\right]^{+}\right)}{dt} = r_{5,L} - r_{6,L} + r_{5,C} - r_{6,C} \tag{15h}$$

$$\frac{d\left(\mathrm{Pc}^{+}\right)}{dt} = 2r_{8,L} - r_{3,L} - r_{5,L} + 2r_{8,C} - r_{3,C} - r_{5,C} \tag{15i}$$

$$\frac{d\left(\mathrm{Pc}\right)}{dt} = r_{3,L} - 2r_{8,L} + r_{5,L} + r_{3,C} - 2r_{8,C} + r_{5,C} \tag{15j}$$

$$\frac{d\left(\mathrm{PSI}^{+}\right)}{dt} = -2r_{8,L} + 2r_{9,L} + -2r_{8,C} + 2r_{9,C} \tag{15k}$$

$$\frac{d\left(\mathrm{PSI}\right)}{dt} = 2r_{8,L} - 2r_{9,L} + 2r_{8,C} - 2r_{9,C} \tag{15l}$$

$$\frac{d\left(\mathrm{Fd}^{+}\right)}{dt} = 2r_{10,L} - 2r_{9,L} + 2r_{11,L} + 2r_{10,C} - 2r_{9,C} \tag{15m}$$

$$\frac{d\left(\mathrm{Fd}\right)}{dt} = 2r_{9,L} - 2r_{10,L} - 2r_{11,L} + 2r_{9,C} - 2r_{10,C} \tag{15n}$$

$$\frac{d\left(\mathrm{H_2}\right)}{dt} = r_{10,L} \tag{15o}$$

$$\frac{d\left([\mathrm{CH_2O}]\right)}{dt} = 0.5r_{11,L} - r_R \tag{15p}$$

$$\frac{d\left(\mathrm{H_S}^+\right)}{dt} = -r_{4,L} - r_{6,L} + 2r_{13,L} - r_{4,C} - r_{6,C} + 2r_{11,C} \tag{15q}$$

$$\frac{d\left(\mathrm{H_L}^+\right)}{dt} = r_{4,L} + r_{6,L} - 2r_{13,L} + r_{4,C} + r_{6,C} - 2r_{11,C} \tag{15r}$$